THE GEOLOGICAL SOCIETY OF AMERICA®

Metasediments from the lower crust reveal the history of the Picuris orogeny, southwest USA

Mary F. Ringwood[1†], Roberta L. Rudnick[1,2], and Andrew R.C. Kylander-Clark[1]
[1]*Department of Earth Science and Earth Research Institute, University of California Santa, Barbara, Santa Barbara, California 93106, USA*
[2]*Department of Geology, University of Maryland, College Park, Maryland 20742, USA*

ABSTRACT

Petrologic and geochronologic data for metapelitic lower crustal xenoliths from New Mexico (USA) and Chihuahua (Mexico) states provide evidence for both a magmatic and collisional component to the enigmatic Mesoproterozoic Picuris orogeny. These garnet-sillimanite-bearing metapelites are found within the southern Rio Grande rift at Kilbourne Hole and Potrillo Maar in southern New Mexico and northern Chihuahua. Geothermobarometry and rutile with Quaternary U-Pb dates indicate equilibration in the local lower crust, which is actively undergoing ultra-high temperature (UHT) metamorphism (Cipar et al., 2020). The samples contain older detrital zircons dating back to the Paleoproterozoic, marking their deposition at the surface. Coupled zircon U-Pb dates and trace-element ratios (e.g., Gd/Yb) show a clear transition from oscillatory-zoned, low-Gd/Yb detrital magmatic zircon to featureless, high-Gd/Yb metamorphic zircon between 1500 and 1400 Ma, marking the transition from subduction to collision during this period. Metamorphic zircon and monazite grew in two major intervals. The first, between ca. 1450 and 1350 Ma, documents the journey of the sediments to depth within the orogen and provides evidence of extended Mesoproterozoic metamorphism in the region. The second corresponds with UHT metamorphism that commenced at ca. 32 Ma and is associated with the Rio Grande rift. Whereas nearly all garnets are homogeneous in both major and trace-elements, a single garnet from one sample has a core defined by abundant quartz and acicular sillimanite inclusions. The core and rim of this garnet is homogenous in major and most trace-elements, but the rim is enriched in the slowest diffusing elements, Zr and Hf, which likely indicates rim growth at higher temperatures. We interpret the garnet core to have grown at the time of emplacement of the sediments into the lower crust. Because this occurred in the sillimanite stability field and because the metamorphic zircon and monazite all have negative Eu anomalies, indicating their equilibration with feldspar (stable at depths of <45 km), we conclude that the sediments were not emplaced via subduction and/or relamination of forearc sediments, but were instead metamorphosed under warmer, shallower conditions in an orogenic setting. Collectively, the data point to a collisional orogen during the inferred timing of the Picuris orogeny. These samples may therefore define the location of the Picuris suture zone, a key feature of this orogenic event.

INTRODUCTION

The southern margin of Laurentia, which corresponds to the present-day midcontinent region of North America, was an important locus for the growth of continental crust during the Proterozoic (Fig. 1) (Karlstrom et. al, 2001; Whitmeyer and Karlstrom, 2007). This time period was punctuated by a series of well-documented events: the Yavapai, Mazatzal, and Grenville orogenies (Fig. 1) (e.g., Bowring and Karlstrom, 1990; Rivers, 1997; Eisele and Isachsen, 2001; Bartholomew and Hatcher, 2010; Mulder et al., 2017). Despite extensive work on the tectonics of Proterozoic southern Laurentia, less attention has been paid to activity in the time interval between the Mazatzal and Grenville orogenies. Early research focused on the voluminous evolved magmatic rocks emplaced between 1500 and 1340 Ma (including the granite-rhyolite provinces), which have been ascribed an anorogenic origin (e.g., Anderson, 1983; Anderson and Bender, 1989; Anderson and Morrison, 1992). However, work on a variety of rock types, including metasediments and other deformed units provide evidence for a distinct orogeny during this time: the Picuris (Daniel et al., 2013a; 2013b; Karlstrom et al., 2016). Some have suggested that the Picuris is an along-strike analog to the Baraboo and Pinware orogens of eastern Laurentia (Aronoff et al., 2016; Daniel et al., 2023) and that it may represent the final docking of the Mazatzal terrane (Daniel et al., 2013b).

A major issue in understanding the Picuris orogeny is the lack of an obvious suture zone. The only potential evidence of this feature was identified through Nd isotopic mapping (Bennett and DePaolo, 1987; Bickford et al., 2015), which showed a somewhat diffuse isotopic boundary between ca. 1600 and ca. 1400 Ma crust (the Nd line, Fig. 1). Additional data linking the Nd line to the Picuris orogeny would shed light on a possible relationship between the two. Thus, the study of ca. 1500–1400 Ma rocks, especially those that were metamorphosed during this time, is necessary. In particular, lower crustal rocks, which can record tectonic events and changing pressure-temperature (P-T) conditions, have the potential to provide major insight into the extent, timing, and nature of the tectonics involved in the assembly of Laurentia during this time.

Here, we report petrologic and geochronologic data for metapelitic xenoliths carried by magmas erupted within the Potrillo volcanic field from Kilbourne Hole and Potrillo Maar, which are part of the Rio Grande rift in New Mexico (USA) and Chihuahua (Mexico) states (Padovani and Carter, 1977a; 1977b). The data presented include (1) petrography to identify the most appropriate samples for detailed analyses and provide mineralogical and textural context for analyses; (2) U-Pb dates and trace-element analyses of metamorphic zircon, detrital zircon cores, and monazite to determine the timing of metamorphism, as well as maximum depositional age; and (3) mineral and whole-rock

Mary F. Ringwood https://orcid.org/0000-0001-6916-1791
[†]mringwood@ucsb.edu

 https://doi.org/10.1130/B36836.1; 6 figures; 1 table; 1 supplemental file.

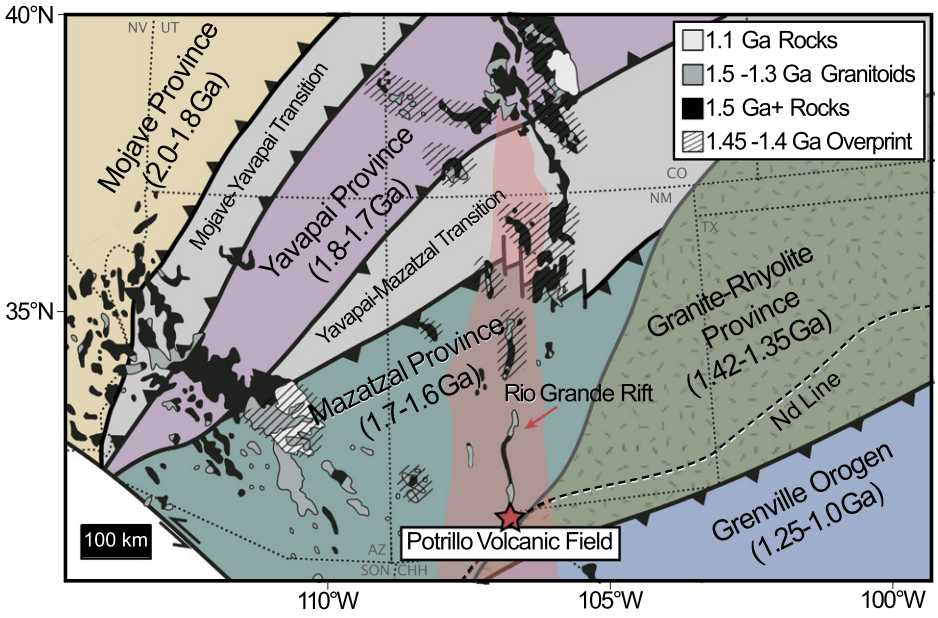

Figure 1. Map of southwest USA showing accreted terranes. Key shows rock outcrops and overprints: locations of 1.5–1.3 Ga granitoids indicated in regions where they occur outside the granite-rhyolite province, the 1.45–1.4 Ga overprint (stippled pattern) shows areas previously identified as having experienced Picuris-aged metamorphism and deformation (Daniel et al., 2013b). Location of Kilbourne Hole and Potrillo Maar marked by star. The Nd line, which marks the boundary determined from Nd isotopic mapping, separates older continental crust (1.8–1.6 Ga Nd model ages) in the north from younger accreted terranes to the south (1.5–1.4 Ga Nd model ages) and is shown as a dashed black line. Rio Grande rift highlighted in red and identified by a red arrow. Modified from Karlstrom et al. (2004), Amato et al. (2008), and Bickford et al. (2015). AZ—Arizona; CHH—Chihuahua (Mexico); CO—Colorado; NV—Nevada; SON—Sonora (Mexico); TX—Texas; UT—Utah.

geochemistry and thermobarometry utilizing the garnet-aluminosilicate-plagioclase-quartz equilibria (GASP) barometer, the Zr-in-rutile barometer, and pseudosection modeling to explore changing metamorphic conditions. The results provide new insights into the nature of the Picuris orogeny and record a lengthy metamorphic history dating back to the Mesoproterozoic.

GEOLOGIC BACKGROUND

Kilbourne Hole and Potrillo Maar are well-known xenolith localities within the Potrillo volcanic field. The lavas erupted during prolonged extension associated with the Rio Grande rift, which has thinned the crust to ~25 km (e.g., Cipar et al., 2020). This area is largely composed of Mazatzal province crust, which makes up much of the southwestern United States and is part of a broader series of terranes accreted during the Meso- and Paleoproterozoic (Fig. 1) (Bowring and Karlstrom, 1990; Rivers, 1997; Karlstrom et al., 2001; Whitmeyer and Karlstrom, 2007). Most Mazatzal crust was generated between 1680 and 1650 Ma, and the terrane likely collided with the Yavapai Province on or near the southern margin of Laurentia during the Mazatzal orogeny, which lasted from 1650 to 1633 Ma. Related post-orogenic magmatism continued until ca. 1600 Ma (Karlstrom et al., 2001; Whitmeyer and Karlstrom, 2007). Most of the region is overlain by Phanerozoic sedimentary and volcanic rocks (Seager et al., 1984).

Following the Mazatzal orogeny, there was a general lull in tectonic activity from 1600 to 1500 Ma, after which time the southern margin of Laurentia was reactivated, producing the granite-rhyolite provinces that are characterized by extensive A-type magmatism lasting from 1500 to 1340 Ma (e.g., Anderson and Bender, 1989; Barnes et al., 2002; Bickford et al., 2015; Holland et al., 2020). Although A-type granitic magmatism is generally interpreted to originate from mantle-derived melts in an anorogenic setting (Frost and Frost, 1997; Frost et al., 2001), evidence for coeval shortening and crustal thickening is indicative of a convergent plate boundary and regional orogenesis (Nyman et al., 1994; Daniel and Pyle, 2006; Bickford et al., 2015). A variety of data point to metamorphism and deformation related to orogenic activity at this time (1500–1400 Ma): detrital zircon U-Pb dates in exposed metasedimentary rocks indicating deposition during the early Picuris and then subsequent deformation (e.g., Daniel et al., 2013a); thrust shear zones in northern New Mexico recording multiple generations of garnet growth between 1460 and 1400 Ma (Aronoff et al., 2016); and metamorphic ages from other minerals like monazite, hornblende, and muscovite (Aronoff et al., 2016; Bollen et al., 2022). Daniel et al. (2013b) originally defined the orogenic activity from 1490 to 1450 Ma as the Picuris orogeny and later expanded this to the Pinware-Baraboo-Picuris orogeny lasting from 1520 to 1340 Ma (Daniel et al., 2023). Magmatism and metamorphism continued until ca. 1340 Ma (Anderson and Bender, 1989; Anderson and Morrison, 1992; Aronoff et al., 2016), indicating that the Picuris orogeny may have been a prolonged event, lasting over 150 Ma and involving both subduction and collision, or could have possibly been a series of discrete, shorter-lived collisional events. While the connection between the A-type magmatism, other granitoids, and regional metamorphism from this time may be unclear, it is now evident that the tectonic setting on the southern margin of Laurentia between 1500 and 1400 Ma included a convergent component and saw a transition from subduction to collision.

Following the Picuris, a shorter magmatic lull lasted until the Grenville orogeny began just to the south (Fig. 1) at ca. 1250 Ma. Grenville activity continued until ca. 980 Ma (Mosher, 1998; Bartholomew and Hatcher, 2010; Mulder et al., 2017) and involved terrane accretion from the modern-day southwest United States through eastern Canada, after which time the crust was relatively stable until the onset of extension in the Late Jurassic (e.g., Bilodeau, 1982; Lawton and McMillan, 1999). Between ca. 150 and 90 Ma the region to the southwest of modern-day New Mexico underwent a transition from an actively rifting margin to a retroarc foreland basin (Lawton et al., 2020). Rifting generated significant uplift along the margins, including the area in southern New Mexico (e.g., Chapman and DeCelles, 2021). Renewed uplift continued during the Laramide orogeny (ca. 80–40 Ma) as a result of shallow angle subduction along the western Laurentian margin (Gastil et al., 1992; Chapman et al., 2020). Post-Laramide, the region was relatively quiet until the Rio Grande rift became active at ca. 32 Ma, which is expressed as extension and magmatism at the surface (Morgan et al., 1986) and ultra-high temperature (UHT) metamorphism in the lower crust (Cipar et al., 2020).

TABLE 1. METAPELITIC XENOLITH SAMPLE INFORMATION

Sample	Locality	Location (°N/°W)	Major phases	Accessory phases	Dated
18KH1	Kilbourne	31.975°/106.967°	40% q, 20% gt, 20% sil, 15% kfs, 5% pl	Rt, ap, zrn, ilm, mnz	Zrn, mnz
18KH9	Kilbourne	31.975°/106.967°	45% q, 20% gt, 20% sil, 15% kfs, < 1% pl	Rt, ap, zrn, ilm, mnz	Zrn, mnz
117848-286	Potrillo	31.769°/106.999°	40% sil, 30% gt, 20% q, 5% kfs, 5% pl	Rt, ap, zrn, ilm, mnz	Zrn, mnz
117848-309	Kilbourne	31.975°/106.967°	45% q, 20% gt, 15% kfs, 15% sil, 5% pl	Rt, ap, zrn, ilm, mnz	Zrn

Notes: ap–apatite; gt–garnet; ilm–ilmenite; kfs–potassium feldspar; mnz–monazite; pl–plagioclase; q–quartz; rt–rutile; sil–sillimanite; zrn–zircon. Modal mineralogy estimated optically. Gt in sample 286 entirely kelyphitized.

SAMPLES AND PREVIOUS INVESTIGATIONS OF XENOLITHS

This study focuses on metapelitic xenoliths (Table 1) from Kilbourne Hole and Potrillo Maar, which are found within the ejecta and surge deposits surrounding the two maars. The samples were either collected by the authors or come from the Ph.D. collection of Elaine Padovani, which is currently curated by the Smithsonian Institution. Specimens contain quartz + sillimanite + garnet + potassium feldspar ± plagioclase ± zircon ± monazite ± rutile ± ilmenite ± apatite ± graphite. No hydrous phases were observed in any of the samples, and many feldspars show perthitic textures or are ternary in nature (data in Supplemental Material[1]), which is indicative of UHT metamorphic conditions (e.g., Elkins and Grove, 1990). The garnets vary in degree of preservation and can contain inclusions of plagioclase, potassium feldspar, sillimanite, zircon, monazite, or quartz. The majority of samples contain garnet that is entirely kelyphite (a fine-grained symplectite of acicular high-Al orthopyroxene + hercynite + glass), which presumably formed from rapid decompression in the host basalt (Padovani and Carter, 1977a; Dégi et al., 2010). Where fresh garnet is preserved, all have kelyphite rims. The rutile in these samples is unique in that some grains are blue in plane-polarized light (or shades of purple, gray, and green in plane polarized light depending on orientation) (Fig. S1).

Padovani and Carter (1977b) estimated that these xenoliths equilibrated between 750 and 1000 °C and 0.6–0.9 GPa, broadly consistent with the deep crust in the region. Furthermore, the seismic P-wave velocity of these xenoliths (calculated to be 6.4–8 km/s; 7 km/s avg.) overlaps the seismic velocity of the local deep crust (Reid et al., 1989; Hamblock et al., 2007).

Early geochronology data for metapelite xenoliths from the Potrillo volcanic field (e.g., Padovani and Reid, 1989; Reid et al., 1989) assumed that the sediments were transported to depth at ca. 1600 Ma, based on Sr, Nd, and Pb isochrons. Scherer et al. (1997) later dated mafic garnet granulites using the Lu-Hf isotope system and identified a major re-equilibration event at ca. 25 Ma, which is consistent with the onset of UHT metamorphism associated with the Rio Grande rift. Scherer et al. (1997) also documented a ca. 1400 Ma inherited zircon from one of these samples, as well as evidence of Cenozoic zircon growth during Rio Grande rift activity. Cipar et al. (2020) dated zircon and rutile from the metasedimentary xenoliths (including sample 18KH9 from this study), as well as calculated Zr-in-rutile and Ti-in-zircon temperatures. The zircon in that study showed Rio Grande rift ages and ultra-high temperatures (>800 °C), and the rutile yielded essentially zero Ma dates (corresponding to eruption <100 ka) and even higher temperatures (>930 °C).

Forty-seven metasedimentary xenoliths were examined in hand specimen and thin section. Of these, four samples were selected for detailed petrochronologic analyses based on the degree of preservation of the garnet, sample size, and representativeness in terms of mineralogy and texture.

METHODS

Major and Trace-Element Analyses of Whole Rocks and Major Minerals

Major-element data for rutile, garnet, and plagioclase were collected using the Cameca SX-100 electron probe micro-analyzer (EPMA) at the University of California Santa Barbara (UCSB), California, USA. Transects of 2 μm spots, spaced 10–20 μm apart, were made across grains, using an accelerating voltage of 15 kV and a beam current of 10 nA. Zirconium contents in rutile were also determined via EPMA. Transects of 5 μm spots, spaced 10–20 μm apart, were done across grains, with an accelerating voltage of 20 kV and a beam current of 80 nA.

Trace-elements in garnet were obtained with either the Agilent quadrupole inductively coupled plasma mass spectrometer (Q-ICP-MS) at UCSB or the ThermoScientific Element2 sector field inductively coupled plasma mass spectrometer (SF-ICP-MS) at California State University Northridge. The Agilent was coupled with a Teledyne CETAC Excimer Excite laser system and the Element2 with a Teledyne CETAC Analyte G2 laser system. 40 μm spots spaced 50 μm apart were used to make transects across grains along the same axes as analyzed by the EPMA. Manganese or Si concentrations from the EPMA were used as the internal element standards, NIST-612 was the calibrating standard, and BHVO-2G and GSD-1G were used as secondary standards (data in Supplemental Material).

Whole-rock major elements were measured on glass beads made by flux fusion of whole-rock powders and analyzed via a Thermo-ARL automated X-ray fluorescence spectrometer (XRF) at Washington State University, Washington, USA, which typically has an uncertainty better than 2% (2σ).

Thermobarometry

Whole-rock major-element data were used to construct pseudosections (Fig. 2) with the Perple_X software (Connolly, 1990) using the internally consistent thermodynamic database of Holland and Powell (2011). Calculations assumed an anhydrous composition based on the lack of hydrous phases in the samples, as well as the extended time over which these samples experienced UHT metamorphism (Cipar et al., 2020).

Zr-in-rutile temperatures were calculated using the Ferry and Watson (2007) and Tomkins and Powell (2007) calibrations of this thermometer. These temperatures were used in conjunction with the garnet-aluminosilicate-plagioclase-quartz equilibria ("GASP") barometer to determine equilibration pressures and temperatures (using THERMOCALC v.3.3: Holland and Powell, 2011; White et al., 2014).

U-Pb Dating and Trace-Element Analyses of Accessory Phases

Zircon was separated from three xenoliths (18KH1, 18KH9, and 117848-286) and mounted in epoxy (zircon was also analyzed in thin section for another well-preserved, but small, sample, 17848-309.). Laser ablation spots were positioned based on cathodoluminescence images

[1]Supplemental Material. Supplemental Data: LASS, EPMA, and XRF data. Supplemental Text: Additional information and figures. Please visit https://doi.org/10.1130/GSAB.S.22087901 to access the supplemental material, and contact editing@geosociety.org with any questions.

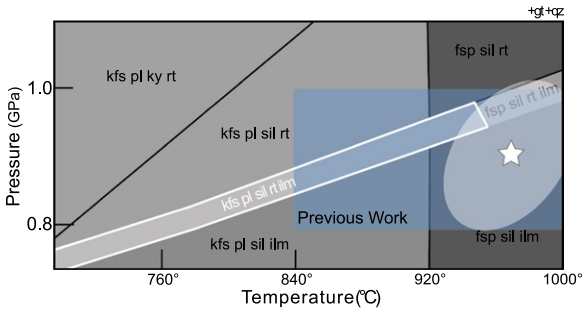

Figure 2. Pseudosection for sample 18KH1, which was collected from Kilbourne Hole: Field outlined in white represents the observed mineral assemblage for the samples studied here. White star shows pressure and temperature obtained from Zr-in-rutile temperature and garnet-aluminosilicate-plagioclase-quartz equilibria barometer, and ellipse around star represents its uncertainty. Blue shading is the range of pressures and temperatures estimated by Padovani and Carter (1977b). All three samples for which X-ray fluorescence (XRF) analyses were obtained yielded the same pseudosection fields within uncertainty. fsp—feldspar; gt—garnet; ilm—ilmenite; kfs—K-feldspar; ky—kyanite; rt—rutile; pl—plagioclase; qz—quartz; sil—sillimanite.

obtained via the FEI Quanta 400f scanning electron microscope at UCSB, and the images were also used to distinguish between oscillatory-zoned igneous/detrital cores and generally featureless metamorphic zircon (Vavra, 1990; Shore and Fowler, 1996).

U-Pb and trace-element data in both detrital and metamorphic zircon were collected simultaneously via laser ablation split-stream ICP-MS (LASS: Kylander-Clark et al., 2013) at UCSB, using either a Nu Plasma or Nu Plasma 3D and an Agilent 7700× quadrupole connected to a Teledyne CETAC Excimer Excite laser system. One sample (117848-309) was not large enough for mineral separates, and so zircon was analyzed in thin section in this case. Initially, 35 μm spots were used, but after determining that there was sufficient U, 12 μm spots were utilized to target the small oscillatory-zoned cores identified in the cathodoluminescence (CL) images (rarely larger than 15 μm in diameter). Metamorphic zircon rims (appearing featureless in CL) were analyzed with 15 μm spots. Reference zircon 91500 was the primary U-Pb standard (1065 Ma: Wiedenbeck et al., 1995), and secondary standards included GJ1 (also the primary trace-element standard; 602 Ma: Jackson et al., 2004), Plešovice (337 Ma: Sláma et al., 2008), R33 (419 Ma: Black et al., 2004), Temora-2 (417 Ma: Black et al., 2004), and Mud Tank (732 Ma: Black and Gulson, 1978). Error propagation follows that outlined in Horstwood et al. (2016), including a typical uncertainty of 1%–2% (2σ) on individual $^{238}U/^{206}Pb$ and $^{207}Pb/^{206}Pb$ ratios (such that the standards produce single populations). Secondary reference materials yielded the following concordia ages (2σ) within 2% of accepted values: GJ1 (597.8 ± 1.4 Ma), Plešovice (336.5 ± 1.2 Ma), R33 (415.7 ± 2.5 Ma), Temora-2 (417.3 ± 2.3 Ma), and Mud Tank (732.2 ± 3.9 Ma). All standard data are provided in the Supplemental Material. Silicon was used as the internal standard for trace-element determinations, assuming a concentration of 14.76%, and external uncertainties for trace-element measurements were generally <10% (2σ). Because of the smaller spot size necessary for targeting specific zircon zones, ~30% of the analyses yielded a 2σ uncertainty of 15% or greater on either the $^{206}Pb/^{238}U$ or $^{207}Pb/^{206}Pb$ ratio; these data generate little to no benefit in geologic interpretation and were thus omitted from further consideration.

Monazite from 18KH1, 18KH9, and 117848-286 was analyzed in thin section for Th-U-Pb ages and select trace-elements via LASS. Analyses were made using 8 μm spots on grains in polished thin sections. Grains were identified through optical microscopy, as well as backscatter electron scans and Ce maps of the thin sections made using the EPMA at UCSB. Th-Pb dates were used for the Rio Grande-rift-age monazite (inset Fig. 3B) to get around the stronger effect of common Pb on younger U-Pb dates. Reference monazite 44069 (424 Ma: Aleinikoff et al., 2006) was the primary U-Pb standard, and secondary standards included Stern (also the primary trace-element standard; 512 Ma: Palin et al., 2013), FC1 (55.7 Ma: Paces and Miller, 1993), and Trebilcock (273 Ma: Tomascak et al., 1996). Error propagation follows that outlined in Horstwood et al. (2016). Secondary reference materials yielded the following concordia ages (2σ) within 2% of accepted values: Stern (503.7 ± 2.2 Ma), FC1 (56.3 ± 0.7 Ma), and Trebilcock (277.1 ± 1.3 Ma). See the Supplemental Material for all standard data. Phosphorous was used as the internal standard for trace-element determinations, assuming a concentration of 12.89%, which is the typical phosphorus concentration in monazite based on the idealized formula. Trace-elements for secondary reference materials reproduce to better than 10% (2σ). Dates with >15% 2σ uncertainty (~30% of the data set) were discarded. No common lead correction was applied to either the zircon or monazite data due to their highly discordant nature.

RESULTS

Mineral and whole-rock compositions used for thermobarometry are reported in the Supplemental Material. Modal mineralogy is provided in Table 1. Pseudosection modeling using the major-element composition of 18KH1 indicates equilibration at 760–965 °C and 0.8–1.0 GPa in the garnet-sillimanite-quartz-potassium feldspar-plagioclase-rutile-ilmenite stability field (Fig. 2). Zr-in-rutile yielded an average temperature of 970 ± 50 °C, corresponding to a pressure of 0.9 ± 0.1 GPa using the GASP barometer (star with surrounding error ellipse in Fig. 2). These values are similar to P-T estimates from previous work (e.g., Padovani and Carter, 1977b; Hamblock et al., 2007; Cipar et al., 2020) and are consistent with equilibration under UHT conditions in the lower crust of the Rio Grande rift, as well as with rutile being open to Pb diffusion at the time of eruption (Cipar et al., 2020).

Over 1000 potential detrital zircon cores were identified in CL images of the grains mounted in epoxy and then analyzed. However, the vast majority of these were strongly discordant (see reasons for this in discussion), and the 12 μm spot size used to collect both U-Pb and trace-element data yielded many analyses with extremely large uncertainties. Approximately 100 analyses of metamorphic zircon were collected from each of the samples shown in Table 1, except for 117848-309, analyses of which were limited by the number of zircon successfully targeted in thin section.

Detrital zircon U-Pb dates (identified by oscillatory zoning in CL) range from ca. 1650–1450 Ma for concordant analyses (data in Supplemental Material) and up to ca. 2500 Ma for discordant analyses (assuming Pb-loss or recrystallization at 16 Ma for the latter; for calculated upper intercept ages and uncertainties based on a 16 Ma lower intercept, see Supplemental Material) (Fig. 3A). The discordant nature of the detrital zircon, as well as their larger uncertainties, makes it difficult to identify a precise maximum depositional age. Featureless metamorphic zircon rims lie on a discordia line between Rio Grande rift dates (≤32 Ma: Morgan et al., 1986; Cipar et al., 2020) and concordant Proterozoic dates between ca. 1450 Ma and 1350 Ma, with eight concordant analyses <1250 Ma (Fig. 3A).

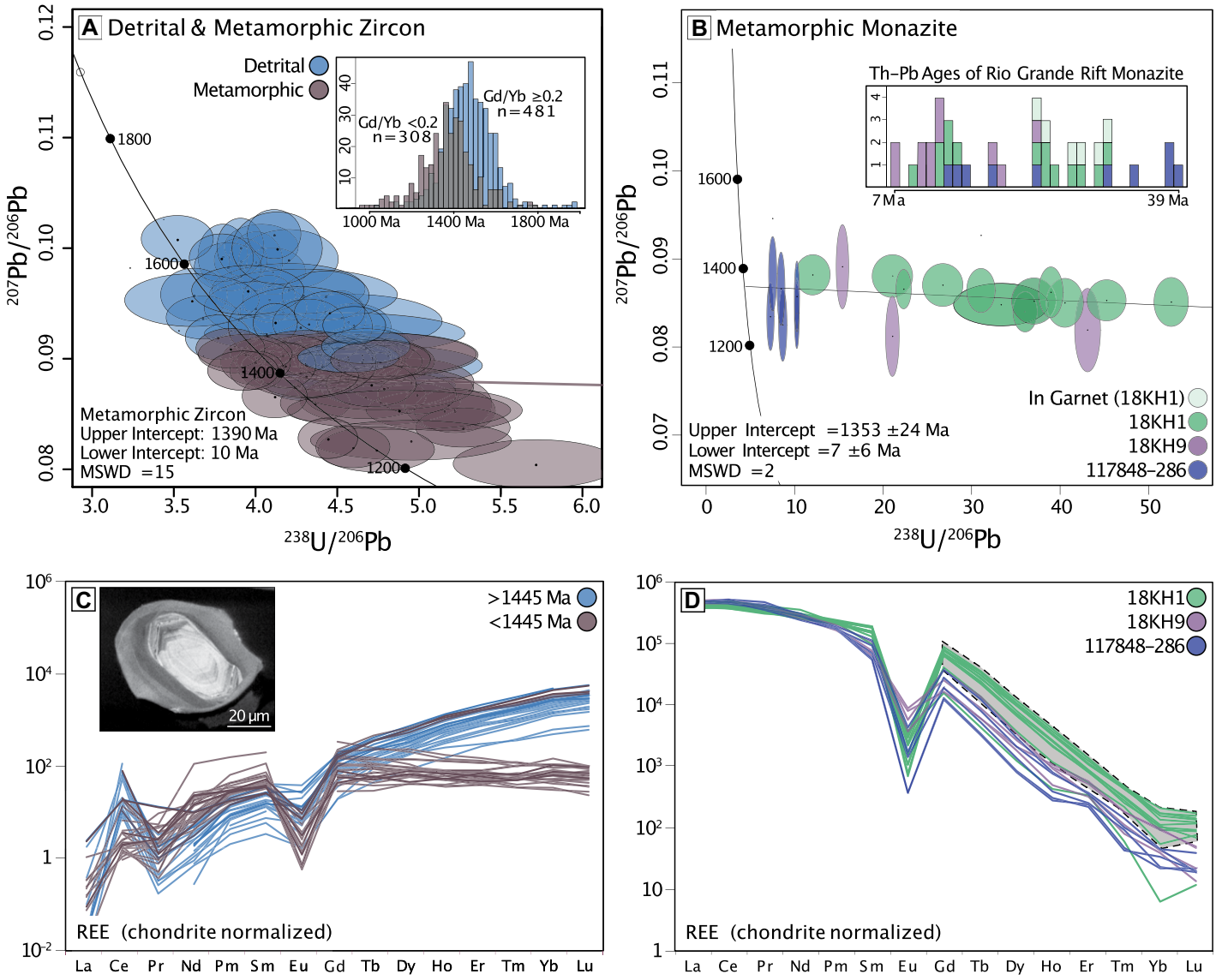

Figure 3. Geochronology results: (A) Tera-Wasserburg concordia plot of detrital zircon cores (n = 45) and metamorphic zircon (n = 33) from the four samples in Table 1 (as determined by cathodoluminescence (CL) images and Gd/Yb ratios) that fall within 15% of concordia and have uncertainties less than 15% (2σ). Inset shows upper intercept ages for each individual zircon with a $^{238}U/^{206}Pb$ ratio <100 classified solely on Gd/Yb ratio (data and associated uncertainties used to make this inset can be found in the Supplemental Material [see footnote 1]). Scale does not show younger ages or the eight analyses >2000 Ma. These data document a clear transition from detrital to metamorphic zircon production during the Picuris orogeny. (B) Tera-Wasserburg concordia plot of metamorphic monazite. All dates are for matrix monazites except for the six pale green data points for sample 18KH1 in the histogram, which are monazites within garnet. Error ellipses show 2σ total uncertainty for individual spot analyses. MSWD—mean square of weighted deviates. (C) Rare earth element (REE) plot for concordant zircon sorted by age, showing a clear transition at 1450 Ma from steep to flat heavy (H)REE. Inset cathodoluminescence image is an example of a zircon from sample 18KH1 with an oscillatory-zoned detrital core surrounded by a metamorphic rim. (D) REE plot of metamorphic monazite. Gray field highlights the higher HREE of the Rio Grande rift-age monazite, indicating these younger grains are not simply the result of Pb loss from Proterozoic monazite and are instead a separate population.

Metamorphic monazite U-Pb and Th-Pb dates also record growth during these time periods (Fig. 3B), with an upper intercept of 1353 ± 24 Ma (2σ) and lower intercept of 7 ± 6 Ma (2σ), though monazite inclusions in garnet (n = 6) yield only Rio Grande rift ages, and the majority of matrix monazite are Rio Grande rift-age (Fig. 3B inset). The Cenozoic monazite have higher heavy rare earth elements (HREE) than the older grains (Fig. 3D), indicating that they are recrystallized grains and not simply Proterozoic monazite that experienced Pb loss. Both the featureless (in CL) metamorphic zircon and the monazite have negative Eu anomalies (Eu/Eu*) and generally flat or depleted HREE, respectively (Figs. 3C and 3D).

Garnets are homogeneous with respect to their major- and trace-element compositions (Fig. 4), which precludes their use in determining the prograde path. Only a single grain (in sample 117848-309) is zoned in Zr and Hf

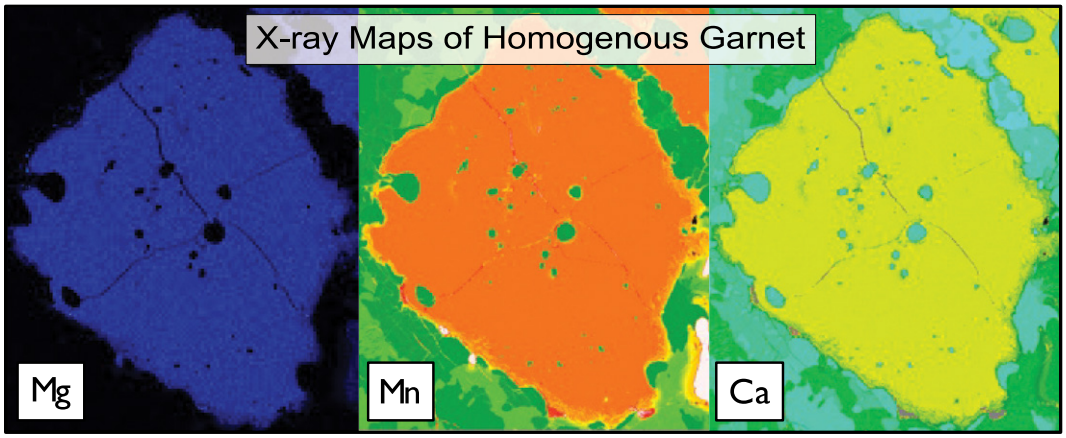

Figure 4. Representative X-ray maps of a chemically homogenous garnet grain from sample 18KH1, a metapelitic xenolith collected at Kilbourne Hole.

(Fig. 5), corresponding to a distinct inclusion-rich core containing fibrous sillimanite, as well as quartz, and an inclusion-poor rim (no dateable phases were found within the core of this garnet). All other garnets in the samples have compositions similar to those of the inclusion-poor rim (including Zr and Hf content). Garnet data are provided in the Supplemental Material, and major-element compositions are plotted in Fig. S4.

DISCUSSION

Timing of Sedimentation and Metamorphism

Detrital and metamorphic zircon were primarily distinguished using CL imaging, assuming oscillatory zoning reflects detrital cores and that featureless zircon grains/rims are metamorphic (see inset to Fig. 3C). Rare earth element patterns (in particular, Gd/Yb ratios) were also utilized to distinguish the two populations and generally correlate with grain structure: Oscillatory zoned (detrital) zircon have low Gd/Yb, and featureless (metamorphic) zircon mostly have high Gd/Yb, indicating equilibration with garnet (e.g., Taylor et al., 2015). Where CL-distinct cores did not clearly show oscillatory zoning, the Gd/Yb ratio was used to determine whether they were detrital or metamorphic.

Most detrital zircon show a large degree of discordancy (Fig. S3), which is likely due to one or more of the following: (1) Pb loss and/or recrystallization during initial and subsequent Proterozoic metamorphic events at ca. 1400 Ma (Picuris orogeny) or ca. 1200 Ma (Grenville orogeny), (2) Pb loss and/or recrystallization during Rio Grande rift UHT metamorphism (Cipar et al., 2020), and/or (3) mixing of detrital/igneous and metamorphic domains in the analysis spot. The last of these was a particular problem due to the small size of most cores, and many analyses aimed at cores incorporated some rim material (This issue was mitigated in Iolite as much as possible, but may not have resulted in removal of all mixed analyses and cannot compensate for inheritance/incomplete recrystallization.). The detrital zircon plotted in Figure 3A represent those that are within 15% of concordia and have uncertainties less than 15% (2σ). These detrital zircon cores mainly record ages corresponding to magmatism associated with the Mazatzal orogeny (>1600 Ma) and early stages of the Picuris orogeny (<1500 Ma). Based on the youngest dates of detrital zircon shown in Figure 3A, the sediments were deposited after 1500 Ma (during the earliest phase of the Picuris).

There is significant overlap in concordant dates of the oscillatory zoned cores and the featureless zircon grains and rims interpreted as metamorphic, which is potentially due to Pb loss from detrital zircon during transport to depth, mixing of these two domains during analysis, and/or uncertainties in individual dates. The inset in Figure 3A shows calculated/restored upper intercept ages for each individual zircon analysis (with $^{238}U/^{206}Pb$ ratios <100) assuming a lower intercept of 16 Ma and sorted by Gd/Yb ratio. We generated this inset image to show the probable upper limit of detrital zircon dates, rather than the transition from detrital to metamorphic zircon. The lower intercept age was chosen because there is a clear discordia between the Mesoproterozoic and Rio Grande rift ages, and 16 Ma is the median age of Rio Grande rift activity (e.g., Cipar et al., 2020).

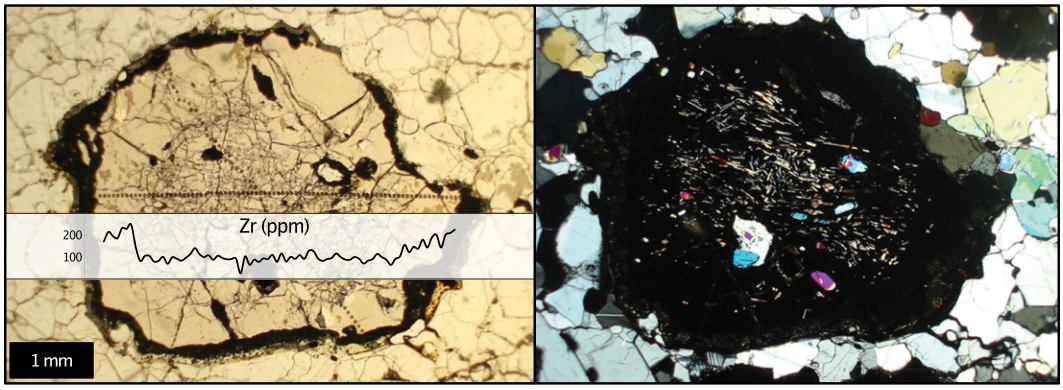

Figure 5. Texturally and chemically zoned garnet with a sillimanite inclusion-rich core indicating metamorphic conditions within the sillimanite field (sample 117848-309, a metapelitic xenolith collected at Kilbourne Hole). Only Zr and Hf preserve chemical zoning, with higher concentrations in the rim, while all other elements are unzoned. Garnet core grew at ~800 °C and rim at ~1050 °C based on the Zr-in-garnet thermometer of Degeling (2002).

With restored ages, the increasing influence of garnet on zircon composition can be seen over time, though the concordant zircon analyses exhibit a significantly more robust relationship between age and Gd/Yb ratio (Fig. 3C).

Metamorphic zircon and monazite yield upper intercept dates primarily between 1450 and 1350 Ma (Fig. 3), which coincides with the Picuris orogeny and records peak metamorphism and therefore the transport of the sediments to depth. There is a clear transition from detrital zircon dates to metamorphic zircon growth at ca. 1450 Ma, which is indicative of a major change in tectonic setting at this time. The metamorphic monazite upper intercept of 1353 ± 24 Ma (discussed below) provides additional evidence for Picuris-aged transport of the samples to depth.

Due to the difficulty in dating very young monazite with the long-lived U-Pb systems, we present the Rio Grande rift-age monazite using their Th-Pb ages (Fig. 3B inset) and the older monazite using the U-Pb systems. The two populations have differing trace-element content, especially in the HREE, indicating that they are likely the product of recrystallization and not simply Pb loss. The ca. 1350 Ma upper intercept may represent mineral crystallization during retrograde metamorphism if it was accompanied by partial melting (e.g., Hacker et al., 2015). Though less likely, this upper intercept may instead show Pb loss during slow cooling, but that would require extended UHT conditions during the Mesoproterozoic, which are not documented in the literature and are difficult to assess using this data set due to the UHT metamorphism associated with the Rio Grande rift. Instead, the spread in metamorphic zircon dates and the monazite upper intercept at ca. 1350 Ma likely reflects an extended period of metamorphism, which is consistent with earlier research that documents protracted metamorphism during the Picuris orogeny (e.g., Aronoff et al., 2016; Bollen et al., 2022). There are also eight nearly concordant (<15% discordancy) metamorphic zircon with upper intercepts of ca. 1250–1000 Ma (out of a total of over 300 high Gd/Yb analyses). These are interpreted to reflect metamorphism associated with the Grenville orogeny, which occurred just to the south (Fig. 1) and would have likely affected the deep crust below the modern Potrillo volcanic field.

Although the recent UHT metamorphism makes interpretation of the Proterozoic history of these rocks challenging, the data presented here demonstrate that the sediments accumulated at the surface before eventually being transported to depth at ca. 1450 Ma, with metamorphism likely extending to ca. 1350 Ma (monazite upper intercept). This time interval corresponds to the Picuris orogeny, which was most recently defined by Daniel et al. (2023) as 1500–1340 Ma in modern southwest USA.

P-T-time Path of the Sediments and Tectonic Setting

Understanding how the metapelites were transported to the lower crust has important implications for interpreting the nature of the Picuris orogeny and its role in the assembly of Laurentia. Several processes may transport sediments to the lower crust: (1) forearc thrusting/underplating of oceanic sediments in a subduction zone (e.g., Pelona-Orocopia-Rand schists, western USA: Jacobson et al., 2011), (2) deep-seated thrust faulting on the continental/inboard side of an arc (retroarc) undergoing crustal shortening (e.g., North American cordillera: DeCelles et al., 2009; Chin et al., 2013), (3) deep-seated thrust faulting in a continent-continent collision zone after subduction ceases (e.g., Himalayas: Zhao et al., 1993), and (4) relamination, wherein buoyant diapirs of subducted continental crust and/or sediments rise through the mantle wedge to the base of the lower crust (e.g., Hacker et al., 2011; Kelemen and Behn, 2016). The petrochronologic data reported here can be used to distinguish between these different scenarios and provide important insight into the tectonic processes responsible for sediment emplacement at depth, as well as evidence for the tectonic setting at the time.

The transport of sediments to the lower crust could only have been achieved in a contractional setting via one of the scenarios previously discussed, thereby providing strong evidence for a major orogenic event at this time. This is consistent with previous work concluding that there was accretion of new crust south of the Nd line (Bickford et al., 2015), which divides older crust to the north and younger to the south, and has long been suspected as an important crustal boundary. The Picuris orogeny partly coincided with mantle-dominated A-type magmatic activity (the extensive granite-rhyolite provinces) (Fig. 1; Bickford et al., 2015, and references therein). Previous work suggests that subduction during the Picuris ceased mid-1400s Ma (e.g., Daniel et al., 2013a; Karlstrom et al., 2016) and that slab breakoff or lower crustal foundering may have occurred, thereby potentially generating the A-type magmatic rocks from this period (Karlstrom et al., 2016). Subduction ceasing at mid-1400s Ma is consistent with the transition from igneous to metamorphic zircon production at ca. 1450 Ma and the onset of monazite growth at ca. 1350 Ma seen in the Potrillo metapelites.

The trace-element composition of accessory phases in the deep crustal metapelites provides clues about the nature of coexisting metamorphic minerals. HREE depletion in metamorphic monazite and zircon indicates growth in the presence of garnet (Rubatto et al., 2013; Taylor et al., 2015). Both phases also have negative Eu anomalies, indicating growth within the feldspar stability field (e.g., Rubatto et al., 2013; Dumond et al., 2015) and therefore at crustal depths, ruling out the higher pressures expected for subduction into the mantle followed by diapiric ascent and relamination (Hacker et al., 2011).

The rim of the single zoned garnet matches the inclusion-poor appearance and Zr and Hf contents of other garnet in these samples (Fig. 4). Thus, the rim is likely Rio Grande rift-age, and the unique core may be a relict of the original prograde metamorphism that occurred during initial transport of the sediment to depth. If so, the abundant sillimanite in the core records a relatively warm metamorphic field gradient at the time of transport—warmer than expected in forearc subduction settings where kyanite is usually the stable aluminosilicate (see figure 4 in Chapman, 2017). As there are no zircon or monazite inclusions in the garnet core, the hypothesis that this is a relict from the Proterozoic is based on its unique appearance (full of acicular sillimanite inclusions) and Zr and Hf concentrations, which differ from both the rim of the grain as well as the other garnet in the samples we examined. As Zr and Hf are some of the slowest diffusing elements in garnet (e.g., Chakraborty and Ganguly, 1991; Li et al., 2018; Bloch et al., 2020), and the core-rim boundary is relatively sharp (unlike a typical diffusion profile), this zoning likely reflects garnet rim growth. The Zr concentrations are compatible with growth of the core at 800 °C and the rim at 1050 °C (using the Zr-in-garnet thermometer of Degeling, 2002), with the latter temperature being consistent with the UHT metamorphism associated with the Rio Grande rift as determined by Zr-in-rutile thermometry (Cipar et al., 2020; this study) and the presence of ternary feldspars. The 800 °C domain may therefore represent a much earlier metamorphic history.

These lines of evidence suggest transport of the sediments to depth in either a backarc setting or within a continent-continent collision zone. If subduction was no longer active along the margin after the mid-1400s Ma (e.g., Daniel et al., 2013a; Karlstrom et al., 2016), the transport of sediments to the lower crust after this period must have occurred within a continent-continent collision, wherein sediments transported to the base of the overriding plate are inserted into the lower continental crust after removal of the down-going slab through rollback, foundering, or breakoff (Fig. 6). This setting may have been similar to modern-day thick continent-continent collisions or to the hotter, thinner, and more duc-

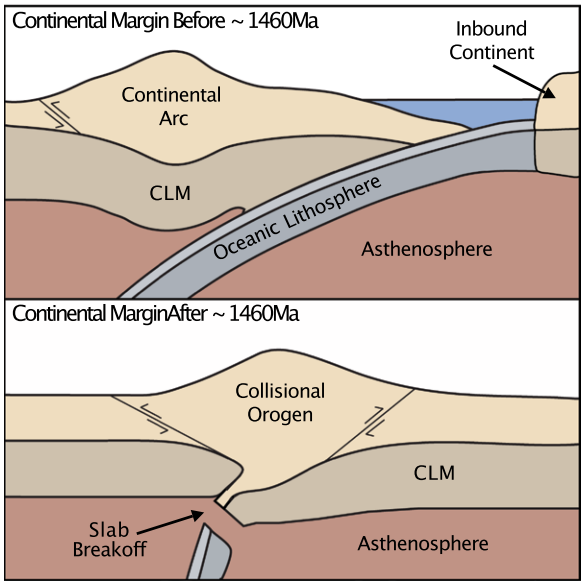

Figure 6. Schematic north-south cross section of the Picuris orogen along what was the Proterozoic southern margin of Laurentia: (A) Before ca. 1460 Ma. (B) Continent-continent collision after ca. 1460 Ma; this date lies within the time window of the transition from detrital/igneous to metamorphic zircon shown in Figure 3A. As the subduction polarity during the Picuris is unknown, it is not possible to determine north from south on the cross section. CLM—continental lithospheric mantle.

tile orogens that may be typical of the Meso- to Paleoproterozoic Earth (Spencer et al., 2021) and which could have involved the transport of sediments to the deep crust through burial and stacking of upper crustal "pop downs" (essentially inverted diapirs: Cagnard et al., 2006). Though this study's data do not provide evidence for the polarity of subduction, the timing of this sequence of events fits with slab breakoff typically occurring after subduction ceases and continent-continent collision begins (e.g., Davies and von Blanckenburg, 1995; van Hunen and Allen, 2011), as well as with the increasing influence of garnet on zircon trace-element contents (Figs. 3A and 3C). If subduction did indeed stop by ca. 1450 Ma, these metasediments were transported to depth within a collisional orogen.

The array of detrital zircon ages (those between 1600 and 1500 Ma) do not match any known sedimentary sequence in the southwest USA (e.g., Daniel et al., 2013a; 2013b; Amato et al., 2018; Amato, 2019). This may be evidence of a non-Laurentian provenance for these sediments, as has been suggested for other rocks in New Mexico (e.g., Piedra Lumbre Formation: Daniel et al., 2013b). In that case, these sediments may have been transported to the southern margin of Laurentia by whatever terrane accreted there during the Picuris orogeny.

CONCLUSIONS

Detrital zircon dates from the metasedimentary xenoliths of the Potrillo volcanic field point to ca. 1650–1450 Ma source rocks, which are distinct from any sedimentary rocks known in New Mexico. The ages of metamorphic zircon and monazite show that the sediments were transported to the lower crust between 1450 and 1350 Ma, during the latter (collisional) part of the Picuris orogeny. The chronology, mineral trace-element data, textural and mineralogical clues, and the fact that it involved the transport of sediments to the deep crust indicate that the Picuris was, indeed, a contractional orogen and not the result of purely extensional or anorogenic activity near the southern margin of Proterozoic Laurentia. Furthermore, the occurrence of these lower crustal metapelites in south-central New Mexico provides corroboration of previous suggestions that the "Nd-line" may represent the location of a suture zone. By providing evidence for the tectonic setting at the time of sediment transport to depth, as well as the possible location of the Picuris suture zone, these data provide insight into an otherwise poorly understood yet major event in the Proterozoic assembly of North America.

ACKNOWLEDGMENTS

We thank Francisco Apen, Brad Hacker, John Cottle, Judy Pu, Elizabeth Erickson, Amy Moser, Christopher Daniel, Chris Andronicus, Harold Stowell, and Ruth Aronoff for their discussions and comments on drafts of this manuscript; Gareth Seward for help with the electron probe micro-analyzer work; Joshua Schwartz for access to the California State University Northridge laser ablation lab where garnet trace-element profiles were analyzed; Elizabeth Anthony at the University of Texas at El Paso for advice and guidance in the field; Jeff Amato, Pat Bickford, and Emily Chin for their insightful feedback as reviewers; Associate Editor Peter Luff for his helpful feedback; the U.S. Bureau of Land Management for giving permission to collect samples at the Organ Mountains-Desert Peaks National Monument, New Mexico, USA; and especially Leslie Hale and staff at the Smithsonian Institution for providing access to their collection of Potrillo xenoliths originally collected and donated by Elaine Padovani. Funding for this project was provided by the Geological Society of America's Graduate Student Research Grant, the Earth Research Institute at the University of California Santa Barbara, the University of Maryland Department of Geology, and National Science Foundation grant EAR2148886.

REFERENCES CITED

Aleinikoff, J.N., Schenck, W.S., Plank, M.O., Srogi, L.A., Fanning, C.M., Kamo, S.L., and Bosbyshell, H., 2006, Deciphering igneous and metamorphic events in high-grade rocks of the Wilmington complex, Delaware: Morphology, cathodoluminescence and backscattered electron zoning, and SHRIMP U-Pb geochronology of zircon and monazite: Geological Society of America Bulletin, v. 118, p. 39–64, https://doi.org/10.1130/B25659.1.

Amato, J.M., 2019, Detrital zircon ages from Proterozoic, Paleozoic, and Cretaceous clastic strata in southern New Mexico: Rocky Mountain Geology, v. 54, p. 19–32, https://doi.org/10.24872/rmgjournal.54.1.19.

Amato, J.M., Boullion, A.O., Serna, A.M., Sanders, A.E., Farmer, G.L., Gehrels, G.E., and Wooden, J.L., 2008, Evolution of the Mazatzal province and the timing of the Mazatzal orogeny: Insights from U-Pb geochronology and geochemistry of igneous and metasedimentary rocks in southern New Mexico: Geological Society of America Bulletin, v. 120, p. 328–346, https://doi.org/10.1130/B26200.1.

Amato, J.M., Ottenfeld, C.F., and Howland, C.R., 2018, U-Pb geochronology of Proterozoic igneous and metasedimentary rocks in southern New Mexico: Post-collisional S-type granite magmatism, *in* Mack, G., Hampton, B., Witcher, J., Ramos, F., Ulmer-Scholle, D., eds., Las Cruces Country III: New Mexico Geological Society 69th Annual Fall Field Conference Guidebook, p. 137–145.

Anderson, J.L., 1983, Proterozoic anorogenic granite plutonism of North America, *in* Medaris, L.G., Byers, C.W., Mickelson, D.M., Shanks, W.C., eds., Proterozoic Geology: Selected Papers from an International Proterozoic Symposium: Geological Society of America Memoir 161, p. 133–154.

Anderson, J.L., and Bender, E.E., 1989, Nature and origin of Proterozoic A-type granitic magmatism in the southwestern United States of America: Lithos, v. 23, p. 19–52, https://doi.org/10.1016/0024-4937(89)90021-2.

Anderson, J.L., and Morrison, J., 1992, Chapter 7 the role of anorogenic granites in the Proterozoic crustal development of North America, *in* Condie, K., ed., Proterozoic crustal evolution: Amsterdam, Netherlands, Elsevier, v. 10, p. 263–299, https://doi.org/10.1016/S0166-2635(08)70121-X.

Aronoff, R.F., Andronicos, C.L., Vervoort, J.D., and Hunter, R.A., 2016, Redefining the metamorphic history of the oldest rocks in the southern Rocky Mountains: Geological Society of America Bulletin, v. 128, p. 1207–1227, https://doi.org/10.1130/B31455.1.

Barnes, M.A., Anthony, E.Y., Williams, I., and Asquith, G.B., 2002, Architecture of a 1.38–1.34 Ga granite-rhyolite complex as revealed by geochronology and isotopic and elemental geochemistry of subsurface samples from west Texas, USA: Precambrian Research, v. 119, p. 9–43, https://doi.org/10.1016/S0301-9268(02)00116-X.

Bartholomew, M.J., and Hatcher, R.D., 2010, The Grenville orogenic cycle of southern Laurentia: Unraveling sutures, rifts, and shear zones as potential piercing points for Amazonia: Journal of South American Earth Sciences, v. 29, p. 4–20, https://doi.org/10.1016/j.jsames.2009.08.007.

Bennett, V.C., and DePaolo, D.J., 1987, Proterozoic crustal history of the western United States as determined by neodymium isotopic mapping: Geological Society of America Bulletin, v. 99, p. 674–685, https://doi.org/10.1130/0016-7606(1987)99<674:PCHOTW>2.0.CO;2.

Bickford, M.E., van Schmus, W.R., Karlstrom, K.E., Mueller, P.A., and Kamenov, G.D., 2015, Mesoproterozoic-trans-Laurentian magmatism: A synthesis of continent-wide age distributions, new SIMS U-Pb ages, zircon saturation temperatures, and Hf and Nd isotopic

compositions: Precambrian Research, v. 265, p. 286–312, https://doi.org/10.1016/j.precamres.2014.11.024.

Bilodeau, W.L., 1982, Tectonic models for Early Cretaceous rifting in southeastern Arizona: Geology, v. 10, p. 466–470, https://doi.org/10.1130/0091-7613(1982)10<466:TMFECR>2.0.CO;2.

Black, L.P., and Gulson, B.L., 1978, The age of the Mud Tank Carbonatite, Strangeways Range, Northern territory: BMR Journal of Australian Geology and Geophysics, v. 3, p. 227–232.

Black, L.P., Kamo, S.L., Allen, C.M., Davis, D.W., and Aleinikoff, J.N., 2004, Improved $^{206}Pb/^{238}U$ microprobe geochronology by the monitoring of a trace-element-related matrix effect; SHRIMP, ID-TIMS, ELA-ICP-MS and oxygen isotope documentation for a series of zircon standards: Chemical Geology, v. 205, no. 1–2, p. 115–140, https://doi.org/10.1016/j.chemgeo.2004.01.003.

Bloch, E.M., Jollands, M.C., Devoir, A., Bouvier, A.S., Ibañez-Mejia, M., and Baumgartner, L.P., 2020, Multispecies diffusion of yttrium, rare earth elements and hafnium in garnet: Journal of Petrology, v. 61, p. 1–29, https://doi.org/10.1093/petrology/egaa055.

Bollen, E.M., Stowell, H.H., Aronoff, R.F., Stotter, S., Daniel, C.G., McFarlane, C.R.M., and Vervoort, J.D., 2022, Reconciling garnet Lu-Hf and Sm-Nd, and monazite U-Pb ages for a prolonged metamorphic event, northern New Mexico: Journal of Petrology, v. 63, no. 5, https://doi.org/10.1093/petrology/egac031.

Bowring, S.A., and Karlstrom, K.E., 1990, Growth, stabilization, and reactivation of Proterozoic lithosphere in the southwestern United States: Geology, v. 18, p. 1203–1206, https://doi.org/10.1130/0091-7613(1990)018<1203:GSAROP>2.3.CO;2.

Cagnard, F., Brun, J.P., and Gapais, D., 2006, Modes of thickening of analogue weak lithospheres: Tectonophysics, v. 421, p. 145–160, https://doi.org/10.1016/j.tecto.2006.04.016.

Chakraborty, S., and Ganguly, J., 1991, Compositional zoning and cation diffusion in garnets, *in* Ganguly, J., ed., Diffusion, Atomic Ordering, and Mass Transport: Selected Topics in Geochemistry: New York, USA, Springer, p. 120–175, https://doi.org/10.1007/978-1-4613-9019-0_4.

Chapman, A.D., 2017, The Pelona–Orocopia–Rand and related schists of southern California: A review of the best-known archive of shallow subduction on the planet: International Geology Review, v. 59, no. 5-6, p. 664–701, https://doi.org/10.1080/00206814.2016.1230836.

Chapman, A.D., Rautela, O., Shields, J., Ducea, M.N., and Saleeby, J., 2020, Fate of the lower lithosphere during shallow-angle subduction: The Laramide example: GSA Today, v. 30, p. 4–10, https://doi.org/10.1130/GSATG412A.1.

Chapman, J.B., and DeCelles, P.G., 2021, Beveling the Colorado Plateau: Early Mesozoic rift-related flexure explains erosion and anomalous deposition in the southern cordilleran foreland basin: Tectonics, v. 40, https://doi.org/10.1029/2020TC006517.

Chin, E.J., Lee, C.A., Tollstrup, D.L., Xie, L., Wimpenny, J.B., and Yin, Q., 2013, On the origin of hot metasedimentary rocks in the lower crust of continental arcs: Earth and Planetary Science Letters, v. 361, p. 120–133, https://doi.org/10.1016/j.epsl.2012.11.031.

Cipar, J.H., Garber, J.M., Kylander-Clark, A.R.C., and Smye, A.J., 2020, Active crustal differentiation beneath the Rio Grande Rift: Nature Geoscience, v. 13, p. 758–763, https://doi.org/10.1038/s41561-020-0640-z.

Connolly, J.A., 1990, Multivariable phase diagrams: An algorithm based on generalized thermodynamics: American Journal of Science, v. 290, p. 666–718, https://doi.org/10.2475/ajs.290.6.666.

Daniel, C.G., and Pyle, J.M., 2006, Monazite-xenotime thermochronometry and Al2SiO5 reaction textures in the Picuris Range, northern New Mexico: New evidence for a 1450–1400 Ma orogenic event: Journal of Petrology, v. 47, no. 1, p. 97–118, https://doi.org/10.1093/petrology/egi069.

Daniel, C.G., Jones, J.V., and Andronicos, C.L., 2013a, Making the case for the Picuris orogeny: Evidence for a 1500 to 1400 Ma orogenic event in the southwestern United States, *in* The Geological Society of America Field Guide, v. 33, p. 205–235, https://doi.org/10.1130/2013.0033(07).

Daniel, C.G., Pfeifer, L.S., Jones, J.V., McFarlane, C.M., Sciences, E., Rock, L., and Rock, L., 2013b, Detrital zircon evidence for non-Laurentian provenance, Mesoproterozoic (ca. 1490–1450 Ma) deposition and orogenesis in a reconstructed orogenic belt, northern New Mexico, USA: Defining the Picuris orogeny: Geological Society of America Bulletin, v. 125, p. 1423–1441, https://doi.org/10.1130/B30804.1.

Daniel, C.G., Indares, A., Medaris, L.G., Jr., Aronoff, R., Malone, D., and Schwartz, J., 2023, Linking the Pinware, Baraboo, and Picuris orogenies: Recognition of a trans-Laurentian ca. 1520–1350 Ma orogenic belt, *in* Whitmeyer, S.J., Williams, M.L., Kellett, D.A., and Tikoff, B., eds., Laurentia: Turning Points in the Evolution of a Continent: Geological Society of America Memoir 220, https://doi.org/10.1130/2022.1220(11).

Davies, J.H., and von Blanckenburg, F., 1995, Slab breakoff: A model of lithosphere detachment and its test in the magmatism and deformation of collisional orogens: Earth and Planetary Science Letters, v. 129, p. 85–102, https://doi.org/10.1016/0012-821X(94)00237-S.

DeCelles, P.G., Ducea, M.N., Kapp, P., and Zandt, G., 2009, Cyclicity in Cordilleran orogenic systems: Nature Geoscience, v. 2, no. 4, p. 251–257, https://doi.org/10.1038/ngeo469.

Degeling, H.S., 2002, Zircon equilibria in metamorphic rocks [Ph.D. thesis]: Canberra, Australia, The Australian National University, 235 p.

Dégi, J., Abart, R., Török, K., Bali, E., Wirth, R., and Rhede, D., 2010, Symplectite formation during decompression induced garnet breakdown in lower crustal mafic granulite xenoliths: Mechanisms and rates: Contributions to Mineralogy and Petrology, v. 159, p. 293–314, https://doi.org/10.1007/s00410-009-0428-z.

Dumond, G., Goncalves, P., Williams, M.L., and Jercinovic, M.J., 2015, Monazite as a monitor of melting, garnet growth and feldspar recrystallization in continental lower crust: Journal of Metamorphic Geology, v. 33, p. 735–762, https://doi.org/10.1111/jmg.12150.

Eisele, J., and Isachsen, C.E., 2001, Crustal growth in southern Arizona: U-Pb geochronologic and Sm-Nd isotopic evidence for addition of the Paleoproterozoic Cochise block to the Mazatzal province: American Journal of Science, v. 301, p. 773–797, https://doi.org/10.2475/ajs.301.9.773.

Elkins, L.T., and Grove, T.L., 1990, Ternary feldspar experiments and thermodynamic models: The American Mineralogist, v. 75, p. 544–559.

Ferry, J., and Watson, E., 2007, New thermodynamic models and revised calibrations for the Ti-in-zircon and Zr-in-rutile thermometers: Contributions to Mineralogy and Petrology, v. 154, p. 429–437, https://doi.org/10.1007/s00410-007-0201-0.

Frost, B.R., Barnes, C.G., Collins, W.J., Arculus, R.J., Ellis, D.J., and Frost, C.D., 2001, A geochemical classification for granitic rocks: Journal of Petrology, v. 42, p. 2033–2048, https://doi.org/10.1093/petrology/42.11.2033.

Frost, C.D., and Frost, B.R., 1997, Reduced rapakivi-type granites: The tholeiite connection: Geology, v. 25, p. 647–650, https://doi.org/10.1130/0091-7613(1997)025<0647:RRTGTT>2.3.CO;2.

Gastil, G., Wracher, M., Strand, G., Lee Kear, L., Eley, D., Chapman, D., and Anderson, C., 1992, The tectonic history of the southwestern United States and Sonora, Mexico, during the past 100 My: Tectonics, v. 11, p. 990–997, https://doi.org/10.1029/92TC00596.

Hacker, B.R., Kelemen, P.B., and Behn, M.D., 2011, Differentiation of the continental crust by relamination: Earth and Planetary Science Letters, v. 307, p. 501–516, https://doi.org/10.1016/j.epsl.2011.05.024.

Hacker, B.R., Kylander-Clark, A.R.C., Holder, R., Andersen, T.B., Peterman, E.M., Walsh, E.O., and Munnikhuis, J.K., 2015, Monazite response to ultrahigh-pressure subduction from U-Pb dating by laser ablation split stream: Chemical Geology, v. 409, p. 28–41, https://doi.org/10.1016/j.chemgeo.2015.05.008.

Hamblock, J.M., Andronicos, C.L., Miller, K.C., Barnes, C.G., Averill, M.G., and Anthony, E.Y., 2007, A composite geologic and seismic profile beneath the southern Rio Grande rift, New Mexico, based on xenolith mineralogy, temperature, and pressure: Tectonophysics, v. 442, p. 14–48, https://doi.org/10.1016/j.tecto.2007.04.006.

Holland, M.E., Grambling, T.A., Karlstrom, K.E., Jones, J.V., Nagotko, K.N., and Daniel, C.G., 2020, Geochronologic and Hf-isotope framework of Proterozoic rocks from central New Mexico, USA: Formation of the Mazatzal crustal province in an extended continental margin arc: Precambrian Research, v. 347, https://doi.org/10.1016/j.precamres.2020.105820.

Holland, T.J.B., and Powell, R., 2011, An improved and extended internally consistent thermodynamic dataset for phases of petrological interest, involving a new equation of state for solids: Journal of Metamorphic Geology, v. 29, p. 333–383, https://doi.org/10.1111/j.1525-1314.2010.00923.x.

Horstwood, M.S.A., Košler, J., Gehrels, G., Jackson, S.E., McLean, N.M., Paton, C., Pearson, N.J., Sircombe, K., Sylvester, P., Vermeesch, P., Bowring, J.F., Condon, D.J., and Schoene, B., 2016, Community-derived standards for LA-ICP-MS U-(Th-)Pb geochronology: Uncertainty propagation, age interpretation and data reporting: Geostandards and Geoanalytical Research, v. 40, p. 311–332, https://doi.org/10.1111/j.1751-908X.2016.00379.x.

Jackson, S.E., Pearson, N.J., Griffin, W.L., and Belousova, E.A., 2004, The application of laser ablation-inductively coupled plasma-mass spectrometry to in situ U-Pb zircon geochronology: Chemical Geology, v. 211, p. 47–69, https://doi.org/10.1016/j.chemgeo.2004.06.017.

Jacobson, C.E., Grove, M., Pedrick, J.N., Barth, A.P., Marsaglia, K.M., Gehrels, G.E., and Nourse, J.A., 2011, Late Cretaceous–early Cenozoic tectonic evolution of the southern California margin inferred from provenance of trench and forearc sediments: Geological Society of America Bulletin, v. 123, p. 485–506, https://doi.org/10.1130/B30238.1.

Karlstrom, K.E., Ahall, K.I., Harlan, S.S., Williams, M.L., McLelland, J., and Geissman, J.W., 2001, Long-lived (1.8–1.0 Ga) convergent orogen in southern Laurentia, its extensions to Australia and Baltica, and implications for refining Rodinia: Precambrian Research, v. 111, p. 5–30, https://doi.org/10.1016/S0301-9268(01)00154-1.

Karlstrom, K.E., Amato, J.M., Williams, M.L., Heizler, M., Shaw, C.A., Read, A.S., and Bauer, P., 2004, Proterozoic tectonic evolution of the New Mexico region: A synthesis, *in* Mack, G.H., and Giles, K.A., eds., The Geology of New Mexico: A Geologic History: New Mexico Geological Society Special Publication 11, p. 1–34.

Karlstrom, K.E., Williams, M.L., Heizler, M.T., Holland, M.E., Grambling, T.A., and Amato, J.M., 2016, U-Pb Monazite and $^{40}Ar/^{39}Ar$ data supporting polyphase tectonism in the Manzano Mountains: A record of both the Mazatzal (1.66–1.60 Ga) and Picuris (1.45 Ga) Orogenies: Socorro, New Mexico, USA, New Mexico Geological Society, p. 177–184, https://doi.org/10.56577/FFC-67.177.

Kelemen, P.B., and Behn, M.D., 2016, Formation of lower continental crust by relamination of buoyant arc lavas and plutons: Nature Geoscience, v. 9, p. 197–205, https://doi.org/10.1038/ngeo2662.

Kylander-Clark, A.R.C., Hacker, B.R., and Cottle, J.M., 2013, Laser-ablation split-stream ICP petrochronology: Chemical Geology, v. 345, p. 99–112, https://doi.org/10.1016/j.chemgeo.2013.02.019.

Lawton, T.F., and McMillan, N.J., 1999, Arc abandonment as a cause for passive continental rifting: Comparison of the Jurassic Mexican Borderland rift and the Cenozoic Rio Grande rift: Geology, v. 27, no. 9, p. 779–782, https://doi.org/10.1130/0091-7613(1999)027<0779:AAACF>2.3.CO;2.

Lawton, T.F., Amato, J.M., Machin, S.E.K., Gilbert, J.C., and Lucas, S.G., 2020, Transition from Late Jurassic rifting to middle Cretaceous dynamic foreland, southwestern U.S. and northwestern Mexico: Geological Society of America Bulletin, v. 132, p. 2489–2516, https://doi.org/10.1130/B35433.1.

Li, B., Ge, J., and Zhang, B., 2018, Diffusion in garnet: A review: Geochimica et Cosmochimica Acta, v. 37, p. 19–31, https://doi.org/10.1007/s11631-017-0187-x.

Morgan, P., Seager, R.W.R., and Golombek, M.P., 1986, Cenozoic thermal, mechanical and tectonic evolution of the Rio Grande Rift: Journal of Geophysical Research: Solid Earth, v. 91, p. 6263–6276, https://doi.org/10.1029/JB091iB06p06263.

Mosher, S., 1998, Tectonic evolution of the southern Laurentian Grenville orogenic belt: Geological Society of America Bulletin, v. 110, p. 1357–1375, https://doi.org/10.1130/0016-7606(1998)110<1357:TEOTSL>2.3.CO;2.

Mulder, J.A., Karlstrom, K.E., Fletcher, K., Heizler, M.T., Timmons, J.M., Crossey, L.J., Gehrels, G.E., and Pecha, M., 2017, The syn-orogenic sedimentary record of the Grenville Orogeny in southwest Laurentia: Precambrian Research, v. 294, p. 33–52, https://doi.org/10.1016/j.precamres.2017.03.006.

Nyman, M.W., Karlstrom, K.E., Kirby, E., and Graubard, C.M., 1994, Mesoproterozoic contractional orogeny in western North America: Evidence from ca. 1.4 Ga plutons: Geology, v. 22, p. 901–904, https://doi.org/10.1130/0091-7613(1994)022<0901:MCOIWN>2.3.CO;2.

Paces, J.B., and Miller, J.D.J., 1993, Precise U-Pb ages of Duluth Complex and related mafic intrusions, northeastern Minnesota: Geochronological insights to physical, petrogenetic, paleomagnetic, and tectonomagmatic processes associated with the 1.1 Ga Midcontinent Rift System: Journal of Geophysical Research: Solid Earth, v. 98, p. 13997–14013, https://doi.org/10.1029/93JB01159.

Padovani, E.R., and Carter, J.L., 1977a, Non-equilibrium partial fusion due to decompression and thermal effects in crustal xenoliths, *in* Dick, H.J.B., ed., Magma Genesis 1977; Proceedings of the AGU Chapman Conference on partial melting in the Earth's upper mantle: Department of Geology and Mineral Industries, State of Oregon, Bulletin 86, p. 43–57.

Padovani, E.R., and Carter, J.L., 1977b, Aspects of the deep crustal evolution beneath south central New Mexico, *in* J.G., Heacock, ed., The Earth's Crust: American Geophysical Union, Geophysical Monograph Series, v. 20, p. 19–55, https://doi.org/10.1029/GM020p0019.

Padovani, E.R., and Reid, M.R.,1989, Field guide to Kilbourne Hole maar, Dona Ana County, New Mexico, *in* Chapin, C.E., and Zidek, J., eds., Field excursions to volcanic terranes in the western United States, Vol. 1, Southern Rocky Mountain Region: New Mexico Bureau of Mineral Resources Memoir 46, p. 1974–1979.

Palin, R.M., Searle, M.P., Waters, D.J., Parrish, R.R., Roberts, N.M.W., Horstwood, M.S.A., Yeh, M.-W., Chung, S.-L., and Anh, T.T., 2013, A geochronological and petrological study of anatectic paragneiss and associated granite dykes from the Day Nui Con Voi metamorphic core complex, North Vietnam: Constraints on the timing of metamorphism within the Red River shear zone: Journal of Metamorphic Geology, v. 31, p. 359–387, https://doi.org/10.1111/jmg.12025.

Reid, M.R., Hart, S.R., Padovani, E.R., and Wandless, G.A., 1989, Contribution of metapelitic sediments to the composition, heat production, and seismic velocity of the lower crust of southern New Mexico, U.S.A: Earth and Planetary Science Letters, v. 95, p. 367–381, https://doi.org/10.1016/0012-821X(89)90111-8.

Rivers, T., 1997, Lithotectonic elements of the Grenville Province: Review and tectonic implications: Precambrian Research, v. 86, p. 117–154, https://doi.org/10.1016/S0301-9268(97)00038-7.

Rubatto, D., Chakraborty, S., and Dasgupta, S., 2013, Timescales of crustal melting in the Higher Himalayan Crystallines (Sikkim, eastern Himalaya) inferred from trace element-constrained monazite and zircon chronology: Contributions to Mineralogy and Petrology, v. 165, p. 349–372, https://doi.org/10.1007/s00410-012-0812-y.

Scherer, E.E., Cameron, K.L., Johnson, C.M., Beard, B.L., Barovich, K.M., and Collerson, K.D., 1997, Lu-Hf geochronology applied to dating Cenozoic events affecting lower crustal xenoliths from Kilbourne Hole, New Mexico: Chemical Geology, v. 142, p. 63–78, https://doi.org/10.1016/S0009-2541(97)00076-4.

Seager, W.R., Shafiqullah, M., Hawley, J.W., and Marvin, R.F., 1984, New K-Ar dates from basalts and the evolution of the southern Rio Grande rift: Geological Society of America Bulletin, v. 95, p. 87–99, https://doi.org/10.1130/0016-7606(1984)95<87:NKDFBA>2.0.CO;2.

Shore, M., and Fowler, A.D., 1996, Oscillatory zoning in minerals: A common phenomenon: Canadian Mineralogist, v. 34, p. 1111–1126.

Sláma, J., Košler, J., Condon, D.J., Crowley, J.L., Gerdes, A., Hanchar, J.M., Horstwood, M.S.A., Morris, G.A., Nasdala, L., Norberg, N., Schaltegger, U., Schoene, B., Tubrett, M.N., and Whitehouse, M.J., 2008, Plešovice zircon: A new natural reference material for U-Pb and Hf isotopic microanalysis: Chemical Geology, v. 249, p. 1–35, https://doi.org/10.1016/j.chemgeo.2007.11.005.

Spencer, C.J., Mitchell, R.N., and Brown, M., 2021, Enigmatic mid-Proterozoic orogens: Hot, thin, and low: Geophysical Research Letters, v. 48, p. 1–12, https://doi.org/10.1029/2021GL093312.

Taylor, R.J.M., Harley, S.L., Hinton, R.W., Elphick, S., Clark, C., and Kelly, N.M., 2015, Experimental determination of REE partition coefficients between zircon, garnet and melt: A key to understanding high-T crustal processes: Journal of Metamorphic Geology, v. 33, p. 231–248, https://doi.org/10.1111/jmg.12118.

Tomascak, P.B., Krogstad, E.J., and Walker, R.J., 1996, U-Pb monazite geochronology of granitic rocks from Maine: Implications for late Paleozoic tectonics in the northern Appalachians: The Journal of Geology, v. 104, p. 185–195, https://doi.org/10.1086/629813.

Tomkins, H.S., and Powell, R., 2007, The pressure dependence of the zirconium-in-rutile thermometer: Journal of Metamorphic Petrology, v. 25, p. 703–713, https://doi.org/10.1111/j.1525-1314.2007.00724.x.

van Hunen, J., and Allen, M.B., 2011, Continental collision and slab break-off: A comparison of 3-D numerical models with observations: Earth and Planetary Science Letters, v. 302, p. 27–37, https://doi.org/10.1016/j.epsl.2010.11.035.

Vavra, G., 1990, On the kinematics of zircon growth and its petrogenetic significance: A cathodoluminescence study: Contributions to Mineralogy and Petrology, v. 106, p. 90–99, https://doi.org/10.1007/BF00306410.

Wiedenbeck, M., Allé, P., Corfu, F., Griffin, W.L., Meier, M., Oberli, F., von Quadt, A., Roddick, J.C., and Spiegel, W., 1995, Three natural zircon standards for U-Th-Pb, Lu-Hf, trace element and REE analyses: Geostandards and Geoanalytical Research, v. 19, p. 1–23, https://doi.org/10.1111/j.1751-908X.1995.tb00147.x.

White, R.W., Powell, R., Holland, T.J.B., Johnson, T.E., and Green, E.C.R., 2014, New mineral activity–composition relations for thermodynamic calculations in metapelitic systems: Journal of Metamorphic Petrology, v. 32, p. 261–286, https://doi.org/10.1111/jmg.12071.

Whitmeyer, S.J., and Karlstrom, K.E., 2007, Tectonic model for the Proterozoic growth of North America: Geosphere, v. 3, p. 220–259, https://doi.org/10.1130/GES00055.1.

Zhao, W., Nelson, K.D., Che, J., Quo, J., Lu, D., Wu, C., and Liu, X., 1993, Deep seismic reflection evidence for underthrusting beneath southern Tibet: Nature, v. 366, p. 557–559, https://doi.org/10.1038/366557a0.

Science Editor: Mihai Ducea
Associate Editor: Peter Luffi

Manuscript Received 9 November 2022
Revised Manuscript Received 13 January 2023
Manuscript Accepted 8 February 2023

Printed in the USA

Ringwood, M.F., Rudnick, R.L., and Kylander-Clark, A.R.C., 2023, Metasediments from the lower crust reveal the history of the Picuris orogeny, southwest USA: GSA Bulletin, https://doi.org/10.1130/B36836.1.

Supplemental Material

Table S1. Petrographic Information for All Samples Analyzed.

Supplemental Text. Documentation of blue rutile in samples.

Figure S1. Examples of the blue-type rutile found in sample 286. Panel B is looking down the c-axis.

Figure S2. Nb concentration in rutile grains measured via EPMA and sorted by perceived color.

Figure S3. All zircon U-Pb data collected having <15% uncertainty.

Figure S4. Composition of garnet grains by sample. Dots are averages for individual samples and encompass uncertainties in analyses.

Supplemental Data. LASS, EPMA, and XRF data.

Table 1. PETROGRAPHIC INFORMATION FOR ALL SAMPLES ANALYZED

Sample	Major Phases	Accessory Phases	Notes
18KH1 (K)	gt (20%), q (40%), sil (20%), kfs (15%), pl (<5%)	rt, ap, zrn, mnz, ilm, oxides	Gts mostly unaltered; one of samples in best shape
18KH9 (K)	gt (20%), q (45%), sil (20%), kfs (15%)	rt, ap, zrn, mnz, ilm, oxides	Relatively inclusion-free gts
18KH10 (K)	gt (15%), q (50%), sil (15%), kfs (20%), pl (1%)	rt, ap, zrn, mnz, ilm, sulfides	Gts small (~2mm); intact gt cores; perthitic kfs
117848-125 (K)	gt (20%), q (40%), sil (15%), kfs (20%), pl (<5%)	rRt, ap, mnz, zrn, oxides, sulfides	Only rims of gt altered
117848-136A (K)	gt (25%), q (40%), sil (5%), kfs (20%), pl (4%), bio (1%)	rt, bio, zrn, oxides, pyx, melt	Gts heavily altered; perthitic kfs; symplectites; only sample with biotite (intermingled with pyx and melt?); bio and pyx possibly secondary
117848-286 (P)	gt (30%), q (20%) sil (45%), kfs (5%)	rt, zrn, mnz, ilm, sulfides	Gts mostly altered; blue rutile
117848-309 (K)	gt (15%), q (45%), sil (10%), kfs (15%), pl (10%)	rt, ap, mnz, zrn, ilm, oxides, sulfides	More pl than typical; lots of large relatively intact gt cores

** K = Kilbourne Hole, P = Potrillo Maar. Ap = apatite, bio = biotite, gt = garnet, ilm = ilmenite, kfs = potassium feldspar, mnz = monazite, pl = plagioclase, pyx = pyroxene q = quartz, rt = rutile, sil = sillimanite, zrn = zircon*

II. BLUE RUTILE

Blue rutile was discovered in four of the metapelite samples (Fig. S1), two of which also have typical brown rutile. Both varieties of rutile were analyzed using the Cameca SX-100 electron microprobe (EPMA) at UCSB to determine whether any unusual chemistry could explain the blue color. Magnesium, Al, Si, Fe, Ti, Zr, V, Cr, Nb, Ta were all analyzed.

Rutile have variable Nb contents. The blue grains contain as much as 1.1 wt% Nb, whereas the brown grains all have less than 0.5 wt%. There is also some variation among the blue rutile. The mean and standard deviation of Nb content of the pure blue (e.g., left grain in Fig. 13) is 4990 ± 2320 ppm and ranges from approximately 2100 to 11,000 ppm. However, including all of the blue-type rutile (blue, purple, green, gray), the average Nb content is 4190 ± 2280 ppm. Though there appears to be a difference between the pure blue and other blue-type

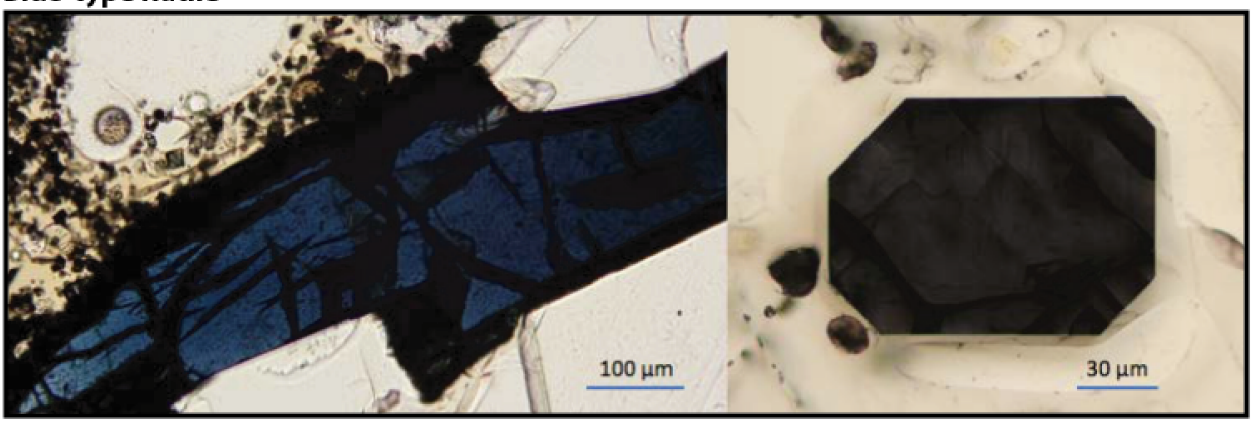

Figure S1. Examples of the blue-type rutile found in sample 286. Panel B is looking down the c-axis.

(e.g., green, purple, etc.) rutile, it is also possible that this is a coincidence and that the color difference is only the result of optic axis orientation. By applying an unpaired t-test to this limited set of data, it was determined that these two populations are not statistically different.

Whereas the brown rutile has an average Nb concentration of 3550 ± 1000 ppm and a maximum measured Nb concentration of < 500 ppm, it is clear that the blue-type rutile can contain significantly more Nb (Fig. S2). However, it is probable that the blue color is not due to the presence of additional Nb. Rather, the two are likely the result of the same thing: the presence of Ti^{3+} in the rutile crystal lattice. While there is only one other documented occurrence of natural terrestrial blue rutile (Mposkos and Kostopoulos, 2001), there are multiple instances of synthetic blue rutile containing Ti^{3+} documented in the materials science literature (e.g., Khomenko et al., 1998). If Ti^{3+} is the cause of the blue color in these rutile, it would be possible to explain the high Nb content by a coupled substitution of Nb^{5+} and Ti^{3+} for $2Ti^{4+}$.

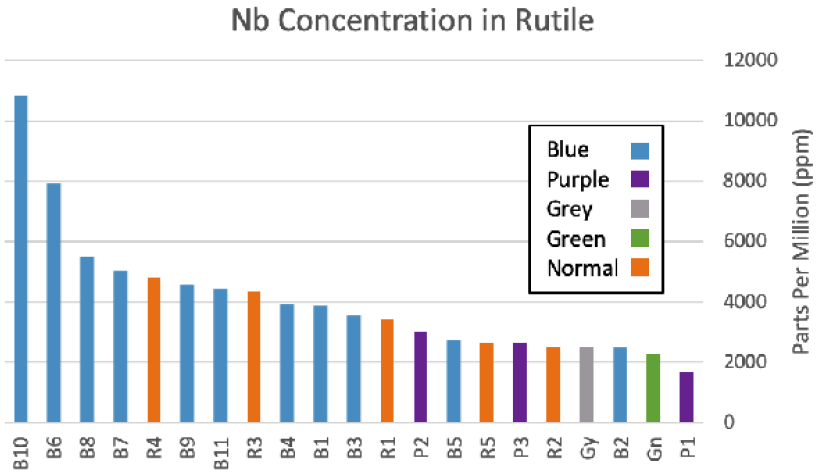

Figure S2. Nb concentration in rutile grains measured via EPMA and sorted by perceived color.

III. ALL ZIRCON DATA

All zircon data collected from the four samples (both detrital and metamorphic) are shown in Fig. S3.

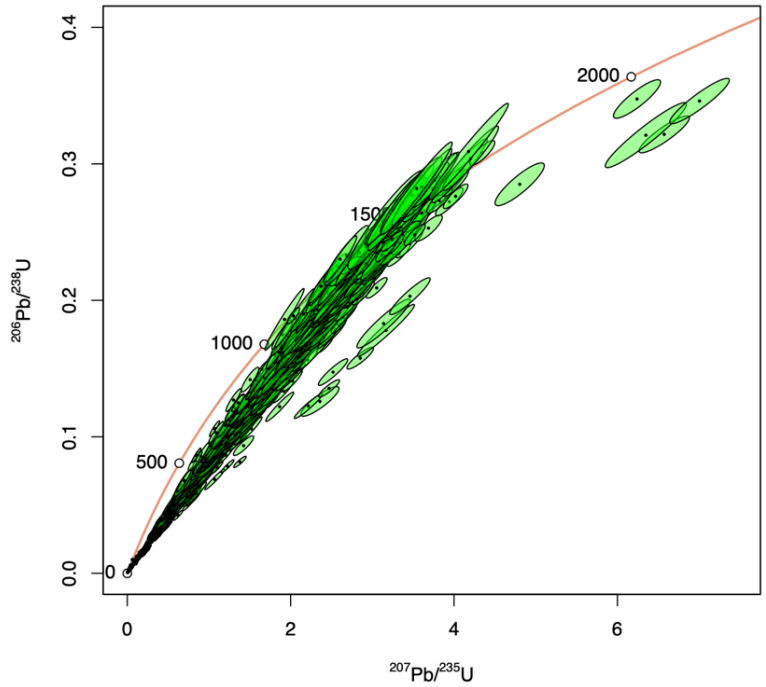

Figure S3. All zircon U-Pb data collected having <15% uncertainty.

IV. GARNET COMPOSITIONS

Samples in supplementary tables have been plotted herein to show composition (Alm-Py-Grs content).

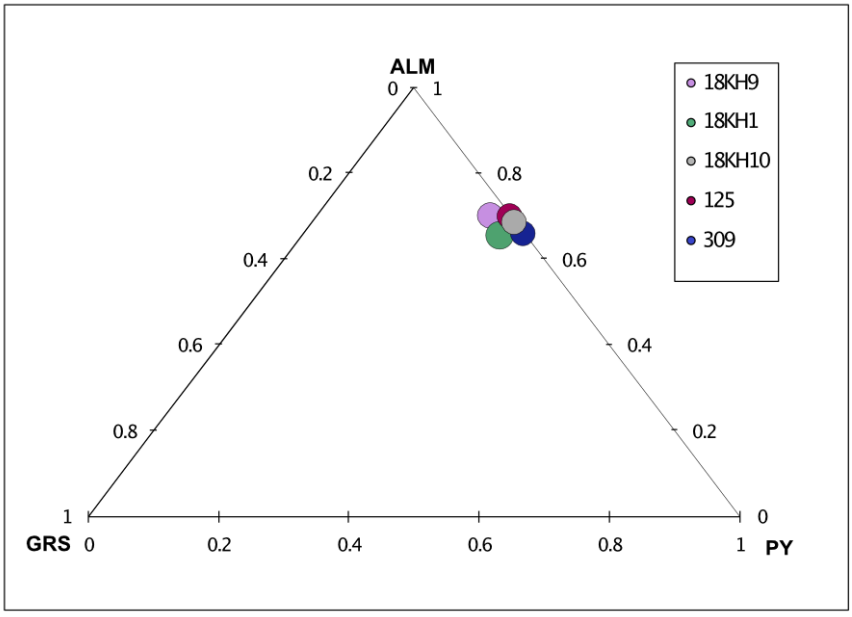

Figure S4. Composition of garnet grains by sample. Dots are averages for individual samples and encompass uncertainty Samples. 125 and 309 are SI samples with the prefix 117848.

V. REFERENCES

Khomenko, V.M., Langer, K., Rager, H., and Fett, A., 1998, Electronic absorption by Ti 3 + ions and electron delocalization in synthetic blue rutile: Physics and Chemistry of Minerals, v. 25, p. 338–346.

Mposkos, E.D., and Kostopoulos, D.K., 2003, Diamond, former coesite and supersilicic garnet in metasedimentary rocks from the Greek Rhodope: a new ultrahigh-pressure metamorphic province established: Earth and Planetary Science Letters, v. 214, p. 675–678, doi:10.1016/S0012-821X(03)00378-9.